JOURNAL OF CATALYSIS 50, 479–493 (1977)

Pt/SiO_2

II. Characterization of the Gel and the Platinum Particles by X-Ray Diffraction

S. R. SASHITAL,[1] J. B. COHEN,[2] R. L. BURWELL, JR., AND J. B. BUTT

Department of Materials Science and Engineering, The Technological Institute, Ipatieff Catalytic Laboratory, and Materials Research Center, Northwestern University, Evanston, Illinois 60201

Received March 7, 1977; revised August 22, 1977

Modern techniques for analysis of X-ray diffraction profiles have been applied to several of the platinum–silica gel catalysts described in Part I to determine average platinum crystallite size, percentage exposed, crystallite shape, size distribution, lattice parameter, residual stresses and strains, presence or absence of faulting, and mean-square amplitude of vibration. In addition the surface area of the gel was determined with small-angle scattering (SAS). There is good agreement between the percentage exposed of platinum measured by gas adsorption in Part I and the results reported here, calculated from crystallite sizes, indicating the crystallite size is the true platinum particle size. Crystallites to sizes as small as ≈25 Å have been examined. Furthermore, the crystallites are equiaxed in shape (and definitely not cuboidal) and are strain and defect free, except in the case where the average size is near the pore size of the gel. Size distributions are sharper when the catalyst preparation is by impregnation rather than by ion exchange. The size distributions indicate that there is coalescence of some surface species during preparation rather than coarsening (Ostwald ripening). The mean-square amplitude of vibration of platinum increases by ≈30% as the particles decrease in size from ≈100 to ≈25 Å. There is no change in the lattice parameter greater than ≈0.1%. The gel surface areas determined by SAS are in agreement with those determined in Part I by physisorbtion of nitrogen.

INTRODUCTION

The wide-angle diffraction pattern has often been utilized to characterize platinum catalysts [see ref. (*1*) for a review]. Either the half-width or the integral breadth of a peak has been employed to obtain a size, but it has not been fully realized that this size is really a ratio of the width of the size distribution, or mean-square size, to the average size, $\langle L^2 \rangle / \langle L \rangle$ (*2*). Furthermore, such techniques inherently require assumptions that the shape of the diffraction profile is a simple function in order to correct for the shape of the peak due to instrumental factors. Often, it has been *assumed* that there are no strains in the crystallites (which also contribute to broadening) or vastly simplified corrections are made for this strain (*3*). It is also commonly believed in the field of catalysis that this technique is not really applicable when average sizes are less then 50 Å.

On the other hand, the advantages of the X-ray technique are that statistical sampling is obtained because of the large

[1] Current address: Hughes Research Laboratories, 3011 Malibu Canyon Road, Malibu, Calif. 90265.

[2] To whom correspondence should be addressed.

ISSN 0021-9517

specimen employed, and specimen preparation is relatively simple. This is in contrast to electron microscopy where considerable effort is necessary to prepare an undisturbed electron-transparent slice and to gather statistically significant data.

From the wide-angle pattern it is possible to obtain the following information with modern X-ray techniques: (i) average crystallite size, (ii) crystallite shape, (iii) stresses, (iv) microstrains (and hence dislocation density), (v) presence of absence of faulting in the particles, (vi) size distribution if the crystallites are strain free (this is often the case as will be shown below), (vii) lattice parameter, and (viii) mean-square amplitudes of vibration.

Item (i) can also be obtained by gas adsorption which is of course, the more common technique, but the X-ray method does not require any assumptions about stoichiometry or equilibrium, and sample cleanliness is less important. However, it is necessary to check that the crystallite size is the true platinum particle size. Items (i), (ii), and (vi) can also be obtained from small-angle scattering (*1, 4*), but it is necessary to completely fill the silica pores with an organic fluid with the same electron density as that of silica gel to eliminate the pore scattering, and this is difficult to maintain.

The techniques employed in this portion of the study are: (a) Fourier analysis of the X-ray diffraction profile [sometimes known as the Warren–Averbach method (*5*)], (b) least-squares studies of peak shifts, and (c) integral intensities of the peaks. These have been extensively tested and employed in the field of metallurgy for the last 20 years (*6*). To date there has been no systematic study of supported catalysts *in situ* with these methods, especially in conjunction with chemical studies (see Parts I (*7*) and III (*8*) of this series). Smith (*9*) studied one platinum–silica gel catalyst and showed that it was strain free. He also examined one palladium–carbon catalyst. Pausescu *et al.* (*10*) dissolved away the support in platinum–alumina catalysts and applied Fourier methods to the residue to obtain mean crystallite sizes and size distributions, but they did not consider whether or not there were strains in the platinum particles contributing to the peak shape. Das *et al.* (*11*) examined platinum black for size (55–75 Å), strain, and faulting. No concurrent chemical studies on the same catalysts were reported in any of these references.

It is the purpose of this paper to demonstrate the usefulness of Fourier techniques by examining some of the catalysts described in Part I (*7*) for items i–viii listed above and to compare the results with percentage exposed by hydrogen chemisorption. The catalysts examined were those prepared as in Part I and stored in air for 1 year or more. It is shown in Part I that O/Pt × 100 was the same as D_h. It will be shown that the platinum core after this exposure to air is unaffected by the oxygen pick-up, through a percentage exposed (of platinum) of 40%.

The work done here employed a computer-controlled conventional diffractometer, and data on platinum sizes as small as ≈25 Å were obtained. With the new high-intensity rotating anode sources, or synchrotron radiation, smaller sizes could be examined even under a suitable atmosphere.

In addition to these studies of the wide-angle pattern from platinum, the surface area of the gel employed to produce the catalysts (and that of two surface area standards that had been examined in several laboratories by gas adsorption techniques) was measured by means of small-angle X-ray scattering.

THEORY

Fourier Analysis

Several reviews now exist concerning the Fourier analysis of peaks in a wide-

angle X-ray powder diffraction pattern (*5*, *6*, *12*), including suitable computer programs (*13*). The diffracted power ($P'_{2\theta}$) at scattering angle 2θ about a peak is represented by a general one-dimensional Fourier series:

$$P'_{2\theta} = K(\theta) \sum_{n=-\infty}^{+\infty} \{G_r(n) \cos 2\pi nh + G_i(n) \sin 2\pi nh\}, \quad (1)$$

where $K(\theta)$ includes such angular dependent factors as the scattering factor and Lorentz and polarization terms. The term $h = (2/\lambda)(\sin\theta - \sin\theta_0)$, where λ is the wavelength of the radiation, 2θ is the measured scattering angle, and $2\theta_0$ is the position of the centroid of the peak.

In order to obtain the diffraction profile due to crystallite size, faults, microstrains, etc., it is necessary to correct the shape for instrumental factors, principally the width of the X-ray source, slit size, and broadening due to penetration of the X-ray beam into the specimen. This can be done by the method of Stokes (*14*). Denoting the Fourier cosine and sine coefficients of a standard (with the same absorption coefficient for X-rays as the sample of interest but with a crystallite size greater than $\approx$2000 Å and no strains) by $F_r(n)$, $F_i(n)$, and the coefficients of the corrected profile as $A_r(n)$, $A_i(n)$:

$$A_r(n) = \frac{G_r(n)F_r(n) + G_i(n)F_i(n)}{[F_r(n)]^2 + [F_i(n)]^2}, \quad (2a)$$

$$A_i(n) = \frac{G_i(n)F_r(n) - F_i(n)G_r(n)}{[F_r(n)]^2 + [F_i(n)]^2}. \quad (2b)$$

This correction also eliminates contributions due to the $K_{\alpha_1} - K_{\alpha_2}$ doublet which is generally present in any diffraction peak (*15*). The Fourier inversion for the coefficients should be carried out about the centroid of each profile (*12*).

The coefficient $A_r(0)$ which represents the area under a peak, should be unity in this formulation by definition, but there is difficulty especially with small particles in a catalyst in establishing the true background due to the large breadth of the peaks, peak overlap, and the scattering from the support. Experimental procedures can minimize these but not eliminate them. By extrapolating $\ln A_r(n)$ vs n (which is linear for small n), a correction for $A_r(0)$ can be obtained which can be employed to correct integrated intensities (*16*).

The Fourier cosine coefficient $A_r(n)$ is really the product of two terms (*2*, *5*), one involving the crystallite size $A_r^s(n)$, and the other microstrains, $A_r^D(n)$.

$$A_r(n) = A_r(n)^s A_r(n)^D, \quad (3a)$$

$$\ln A_r(n) = \ln A_r^s(n) - 2\pi^2\langle\epsilon_L^2\rangle L^2 h_0^2/a^2, \quad (3b)$$

for small L, h_0^2, $\langle\epsilon_L^2\rangle$.

Here a is the true lattice parameter, $\langle\epsilon_L^2\rangle$ is the mean-square strain or width of the strain distribution in a column of length L normal to the diffracting planes, and $L = na_3$ where a_3 is the period of the Fourier analysis determined from the tails of the peak:

$$1 = \frac{2a_3}{\lambda}(\sin\theta_{\text{high-angle tail}} - \sin\theta_{\text{low-angle tail}}). \quad (4)$$

The term h_0^2 is $(h^2 + k^2 + l^2)$, the sum of the Miller indices of the peak. It is a simple matter to obtain the strain from the slope of Eq. (3b) with two or more orders of a peak (200, 400, or 111, 222). It is not possible to use 111, 200, etc., unless the material is elastically isotropic. It is, in fact, sometimes possible to do this entire analysis with a single peak (*17*).

From the extrapolated particle-size coefficients $A_r^s(n)$, the mean effective crystallite size $\langle L_{\text{eff}}\rangle$ can be obtained:

$$\left[\frac{dA_r^s(n)}{dn}\right]_{n\to 0} = -\frac{1}{\langle L_{\text{eff}}\rangle_{hkl}}. \quad (5)$$

TABLE 1

Calculated Particle Sizes $\langle L \rangle$ in $\langle hkl \rangle$ Directions for Different Boundary Faces on a Particle $\{uvw\}$[a]

$\langle L \rangle_{hkl}$	{100}	{110}	{111}
$\langle L \rangle_{111}$	0.58	1.16	1.15
$\langle L \rangle_{100}$	1.00	1.00	1.00
$\langle L \rangle_{110}$	0.71	0.94	1.42
$\langle L \rangle_{311}$	0.66	0.95	1.10

[a] From D. E. Mikkola, Ph.D. Thesis, Northwestern University (1964).

Note that $A_r^s(n)$ is needed for $n \to 0$; i.e., only for small values of n so that Eq. (3b) is satisfactory for obtaining these values.

Care must be taken not to employ $A_r(0)$ or $A_r(1)$ which, as already mentioned, are affected by incorrect positioning of the baseline.

This mean effective crystallite size requires some comment. It includes any contributions due to stacking faults or microtwins in the crystallites. For example, for 111 and 200 peaks from an fcc material like platinum (*2*, *5*),

$$\frac{1}{\langle L_{\text{eff}} \rangle_{111}} = \frac{1}{\langle L \rangle_{111}} + \frac{1.5\alpha + \beta}{a} \frac{(3)^{\frac{1}{2}}}{4}, \tag{6a}$$

$$\frac{1}{\langle L_{\text{eff}} \rangle_{100}} = \frac{1}{\langle L \rangle_{100}} + \frac{1.5\alpha + \beta}{a}. \tag{6b}$$

Here α and β are, respectively, the probabilities of stacking and twin faults in the [111] direction (the inverse of the average number of planes between such faults). These terms can be obtained in other ways from the diffraction pattern (see below), so that the true size in any *hkl* direction, $\langle L \rangle_{hkl}$, can be measured. Even then, this size may be due to subgrains or dislocations in the actual particle. By comparison of the percentage exposed calculated from these sizes, which will be defined here as D_x, and values from gas adsorption, D_h, or by electron microscopy, it is possible to ascertain quickly whether $\langle L \rangle_{hkl}$ is the actual size of the catalytic particles.

From the sizes in different directions the shape of the crystallite can be obtained:

$$\frac{1}{\langle L \rangle_{hkl}} = \langle |\sin \varphi| \rangle / \langle L \rangle_{uvw}, \tag{7a}$$

where $\langle L \rangle_{uvw}$ is the average distance between the bounding planes (uvw) of the crystallite and (*5*):

$$\sin \varphi = \frac{uh + vk + lw}{(u^2 + v^2 + w^2)^{\frac{1}{2}}(h^2 + k^2 + l^2)^{\frac{1}{2}}}. \tag{7b}$$

Different bounding planes are assumed, and for each, the average of sin φ is obtained for all *hkl* planes in the peak in a powder pattern (*hkl*, $\bar{h}kl$, etc.). Ratios of $\langle |\sin \varphi| \rangle$ for different *hkl* peaks can then be compared to the data, $\langle L \rangle_{hkl}$, to determine the shape. Table 1 gives a set of these calculations for some simple indices of faces.

If enough orders (more than two) can be obtained to carry out a better extrapolation than Eq. (3b) (which is only valid for small values of the last term) or if there are no strains in the crystallites:

$$\frac{d^2 A_r^s(n)}{dn^2} \propto p(n), \tag{8}$$

where $p(n)$ is the distribution or crystallites of length na_3 or $\langle L \rangle$. Thus the size distribution can also be obtained, in some circumstances, from the entire specimen under the X-ray beam. This size distribution has been shown to tail toward large sizes if the crystallites result from coalescence, but tail to small sizes if growth occurs by Ostwald ripening, i.e., through diffusion (*18*). Smith (*19*) has also shown that the size distribution will not have a maximum

for certain shapes, so that this result can also be employed to ascertain shape.[3]

The absence of strains can be readily detected because the Fourier coefficients of multiple orders will superimpose [see Eq. (3b); $A_r(n)$ is independent of hkl for $\langle \epsilon_L^2 \rangle = 0$]. When strains are absent, the size and the distribution can be determined by Fourier analysis of a single peak.

Peak Shifts

The shift of a peak compared to a defect-free standard can be written for fcc materials as (*20*):

$$\Delta 2\theta_{hkl} = J_1 \alpha \tan\theta + J_2 \epsilon\theta \tan\theta + J_5 \sigma \tan\theta + J_6 \frac{\Delta a}{a} \tan\theta. \quad (9)$$

The Js are materials constants, ϵ is the change in (111) planar spacing at a stacking fault (of probability α), σ is stress in the diffracting plane, and $(\Delta a/a)$ is any change in lattice parameter. By examining several peaks α, $\alpha\epsilon$, σ, and $(\Delta a/a)$ can be obtained by least squares. This equation is generally employed by subtracting the difference in angle between a peak and its nearest-neighbor peak, with the same difference from a standard without faults or stresses.

The twin fault probability β can be obtained from the displacement of a peak's centroid from its maximum (*21*). In general, the combined effect on the 111 and 200 peaks is employed and this was the case here.

The mean square vibrational amplitude of the platinum atoms $\langle \mu^2 \rangle$ vs particle size was obtained by (*12*) (a) correcting integrated intensities of several peaks for the baseline error (obtained by comparing the actual and extrapolated $A_r(0)$s); (b) correcting for thermal diffuse scattering (TDS) (*22*); (c) correcting for scattering factor, multiplicity, and Lorentz polarization; and (d) obtaining the slope of the logarithm of the corrected integrated intensity vs $\sin^2\theta/\lambda^2$ by least squares. This slope is $16\pi^2\langle \mu^2 \rangle$.

The first five or six peaks (111–400) were employed in the above study. Scattering factors were taken from ref. (*23*), the lattice parameter from ref. (*24*), and the elastic constants for TDS from ref. (*25*).

Surface Areas of Gel

Surface areas were determined by the well-known method of Porod (*26*).

EXPERIMENTAL

Wide-Angle Pattern

The preparation of the gel and the catalysts examined in this study is given in Part I (*7*). The catalysts examined were 40-SiO_2-PtCl-S, 27-SiO_2-IonX-L, 21.5-SiO_2-IonX-L, and 7.1-SiO_2-PtCl-S [see Part I (*7*) for the meaning of these designations]. At least two specimens from each category were analyzed. A specimen was 5×10^{-3} m thick to produce $\approx 90\%$ absorption of the X-ray beam and was prepared by packing in a rectangular plastic sample container with a dilute solution of DUCO cement in acetone. A standard for the Stokes' correction and a reference for peak shifts was obtained from filings of high-purity platinum wire, sieved to less than 80 μm and annealed at 850°C for 9 hr in a vacuum of 10^{-6} Torr in sealed Pyrex tubes. About 6 wt% of this powder was mixed with silica gel and a dilute solution of DUCO cement in acetone. The platinum particles tended to sink to the bottom of the specimen due to the larger density

[3] In this work Smith erroneously suggested that this size distribution cannot be compared to results from electron microscopy. Considering a collection of uniform-size particles, the X-ray results will give a distribution because the beam sees shallow columns at material near edges and corners. Smith felt the microscopist would see only the one true size. But in making sections for the microscope, the uniform particles will also appear to have a whole range of sizes, especially in thin regions of the order of thickness of the particle sizes.

TABLE 2

Surface Area Determinations, Silica Gel

Catalyst	Surface area		R_p[a] (Å)	Pore size[b] (Å)
	Small angle X-ray scattering	Nitrogen adsorption [see Part I (7)]		
SCI-IUPAC-NPL Surface Area Standard TK 800 Code No. 6A/31/21 (two separate specimens)	259 247	286.1 ± 3.5		
SCI-IUPAC-NPL Gasil Silica 1 Code No. 8A/31/232 (two separate specimens)	183 174	165.8 ± 2.1		—
Silica gel used in this study[c]	239 ± 18	285	150 ± 40	140

[a] Porod radius.

[b] From desorption studies; see Part I (7).

[c] Average of six measurements including 200- to 230-mesh and 100- to 120-mesh samples.

compared to the gel. To produce the required thickness, the specimen was prepared in a series of five layers.

The data was obtained with filtered copper K_α radiation on a conventional diffractometer. Wide receiving slits were employed and the divergence was increased from 1 to 4° above $2\theta = 75°$. A scintillation counter was used with a pulse height analyzer set for ≈90% acceptance. Data were obtained by step scanning in increments of 0.2° across peaks or twice these

TABLE 3

Lattice Parameters, Standard Deviation, and Change in Lattice Parameter for Pt/SiO_2 Catalysts

Catalyst[a]	Lattice parameter, (Å)	Standard deviation (±)	$\Delta a/a$[b]
7.1-SiO_2-PtCl-S			
(1)	3.9250	1.96×10^{-4}	3.31×10^{-4}
(2)	3.9230	6.30×10^{-4}	-1.78×10^{-4}
21.5-SiO_2-IonX-L			
(1)	3.9243	1.31×10^{-3}	1.529×10^{-4}
(2)	3.9209	1.8×10^{-3}	-7.13×10^{-4}
27-SiO_2-IonX-S			
(1)	3.9207	8.3×10^{-4}	-7.65×10^{-4}
(2)	3.9199	9.4×10^{-4}	-9.68×10^{-4}
40-SiO_2-PtCl-S	3.9197	4.17×10^{-3}	-1.02×10^{-3}

[a] Two separate specimens for each catalyst, except the last.

[b] Lattice parameter changes obtained by comparison with $a_0 = 3.9239$ Å for bulk Pt (24). The wavelength of copper $K\alpha_{1,2}$ was taken from ref. (23).

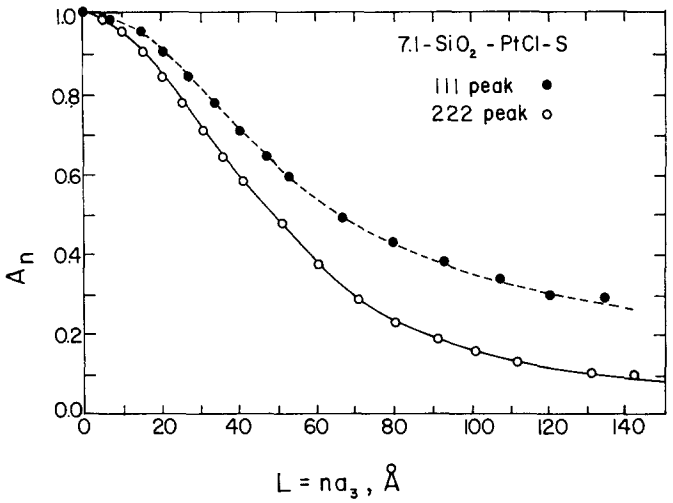

FIG. 1. Stokes'-corrected Fourier coefficients of the 111 and 222 peaks from catalyst 7.1-SiO_2-PtCl-S. Note that the coefficients for the 222 are well below those for the 111, indicating the presence of microstrains.

values for very broad peaks. Times were chosen so that the statistical counting error was always less than 0.3%. The instrument was controlled by a 16K PDP-8E minicomputer [see ref (*27*) for the basic plan of this system].

To properly establish the background, the scattering from the gel alone was measured under identical conditions, from 10° below the first platinum peak to 10° above the last. This data was matched to the data on a catalyst at 9° above the 400 peak from platinum. The match was then within 1.5% of the observed intensity at 9° below the first 111 peak. For Fourier analysis, in regions of peak overlap, such as between the 111 and 200, the peaks were folded from the side without overlap, and extrapolated to the true background.

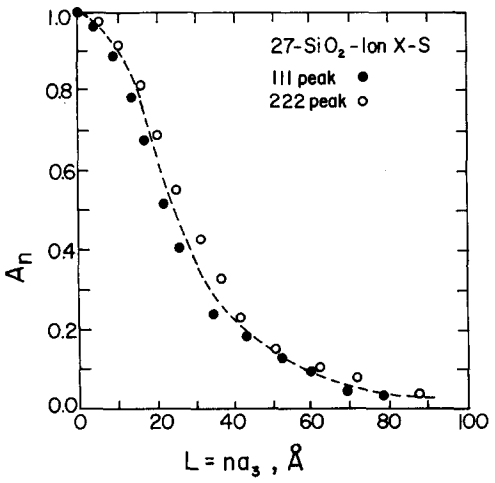

FIG. 2. Stokes'-corrected Fourier coefficients of the 111 and 222 peaks from catalyst 27-SiO_2-IonX-S. The superposition of the coefficients indicates that there are no significant microstrains.

Peak positions were obtained by drawing chords parallel to the background in the top third of the peak and extrapolating their midpoints to the peak's outline. (For the case of unresolved peaks the weighted position $[\frac{2}{3}K_{\alpha_1} + \frac{1}{3}K_{\alpha_2}]$ was employed.) The precision was estimated to be $\pm 0.01°2\theta$ for the first three peaks, $\pm 0.015°2\theta$ for the last three for the two coarser crystallite sizes, and $\pm 0.015°2\theta$ and $\pm 0.025°$ for the two smaller sizes.

Small-Angle Pattern

The small-angle system consisted of an Elliott GX-6 rotating anode generator and a Kratky-type slit (*28*). The data were gathered from about $0.1°2\theta$ to $5\text{–}6°2\theta$ by

repeated scans under minicomputer control so that the statistical error for the lowest count was 3%. Parasitic scattering was obtained (to a statistical counting error of $\leq 5\%$) with the specimen and its holder in the absorber position (before the Kratky slit). All calculations were carried out by the minicomputer program. The gel was dried at 125°C for 2 hr under vacuum while in the holder (which had thin Be windows for the X-rays) and then measured with flowing He purified with a liquid nitrogen cold-trap; tests indicated this drying and He flow were not really necessary.

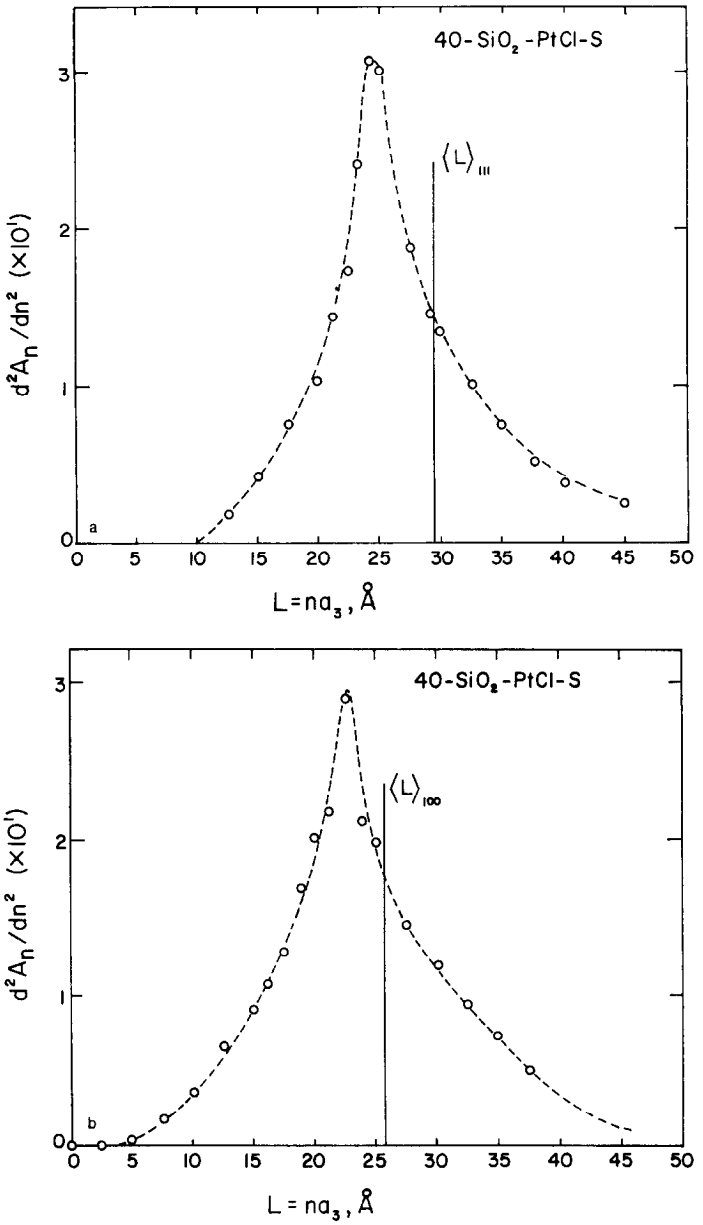

FIG. 3. Particle size distributions for catalyst 40-SiO_2-PtCl-S. (a) ⟨111⟩ direction, (b) ⟨100⟩ direction, (c) ⟨311⟩ direction. Vertical lines indicate mean size.

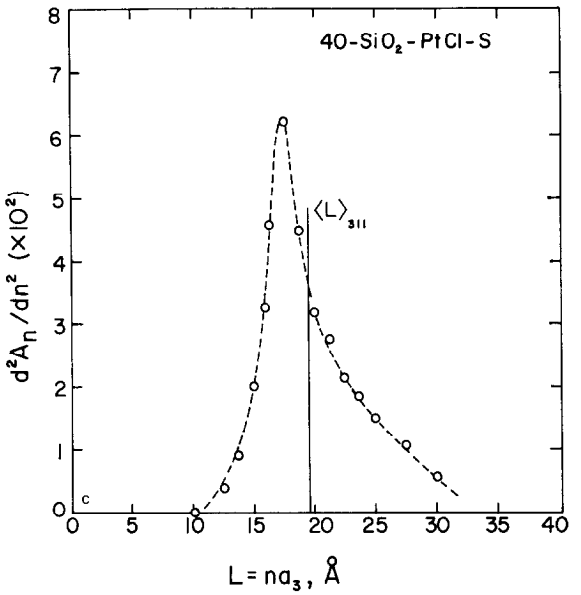

FIGURE 3 (*Continued*)

RESULTS

The data obtained on the gel with small angle scattering are presented in Table 2. The results are in reasonable agreement with those from nitrogen adsorption at −196°C.

The analysis of the platinum diffraction peaks indicates that no measurable faulting or stresses were present; the peak shifts between pairs of peaks were within 1.5 times the sum of the measuring errors (for example, $\Delta 2\theta_{111} - \Delta 2\theta_{200}$ was −.015 to −.03°2θ). Furthermore, from the mean

TABLE 4

Particle Sizes $\langle L\rangle_{hkl}$ in the $\langle hkl\rangle$ Directions and Percentage Exposed

Catalyst[a]	$\langle L\rangle_{111}$ (Å)	$\langle L\rangle_{100}$ (Å)	$\langle L\rangle_{110}$ (Å)	$\langle L\rangle_{311}$ (Å)	D_x (%)	D_h[b] (%)
7.1-SiO_2-PtCl-S[c]						
(1)	131	82	108	81	10	7.1
(2)	111	75	—	—	12	7.1
21.5-SiO_2-IonX-L						
(1)	49	43	45	47	25	21.5
(2)	48	43	45	47	25	—
27-SiO_2-IonX-S						
(1)	43	39	42	31	27	27.3
(2)	40	39	39	39	29	—
40-SiO_2-PtCl-S						
(1)	30	26	22	20	44	39.8
(2)	25	23	—	—	47	

[a] Two separate specimens for each catalyst.

[b] Average of two values from Table 1, Part I (*7*).

[c] There were strains in the Pt particles in this catalyst. The single peak method in ref. (*17*) was employed in this case for the ⟨110⟩ and ⟨311⟩ directions. For the other catalysts, as there was no strain in ⟨111⟩ and ⟨100⟩ directions, this could be assumed for other peaks to obtain the particle size.

crystallite sizes (to be given below) it was possible to calculate the minimum value of the fault probability, assuming only one fault per crystallite. [This is nothing more then the inverse of the number of (111) planes in the length of a crystallite.] The values are 2–20 times *greater* then the measured values. The twin fault probabilities were also negligible, $4–10^{-3}–10^{-7}$, which are well within measuring limits (*29*).

The lattice parameters were therefore evaluated by a least-squares fit measured at the lattice parameter vs the Nelson–Riley parameter (*30*). The results are given in Table 3. There is no indication of any significant change (greater than 0.1%) in

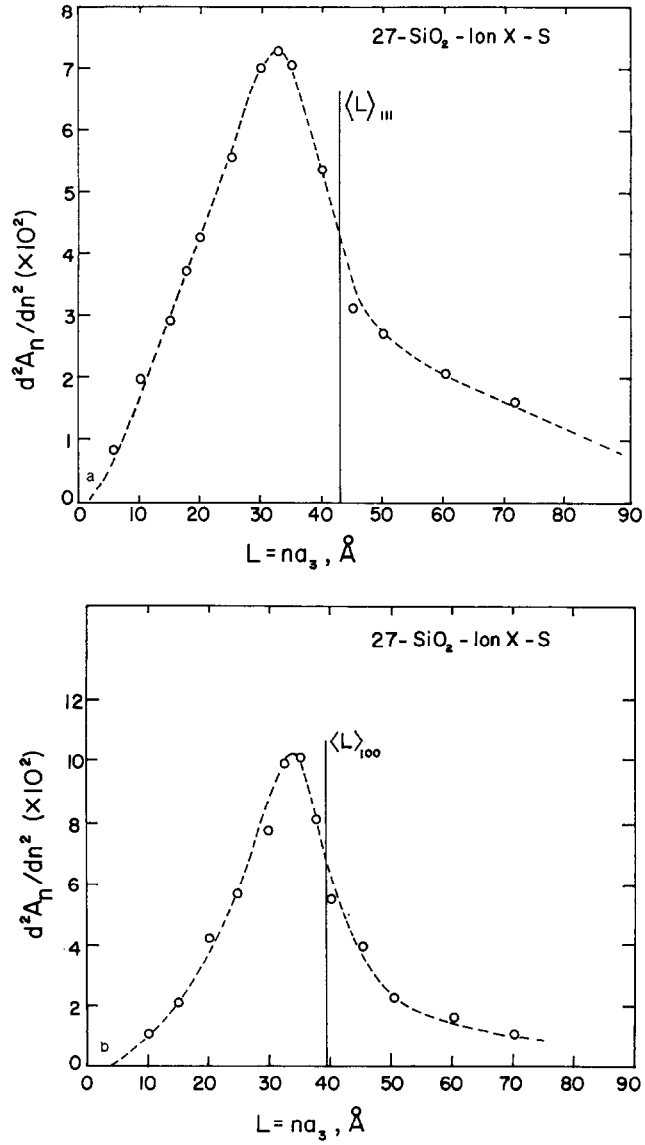

FIG. 4. Particle size distributions for catalyst 27-SiO_2-IonX-S. (a) ⟨111⟩ direction, (b) ⟨100⟩ direction, (c) ⟨311⟩ direction.

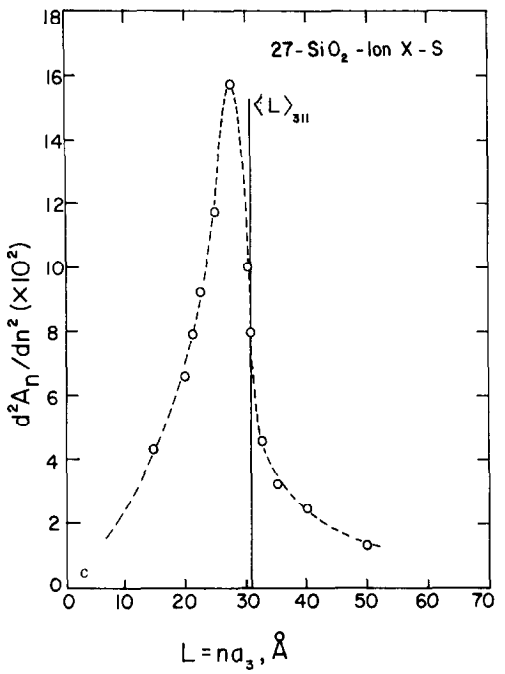

FIGURE 4 (*Continued*)

lattice parameter with platinum crystallite size: The differences from bulk platinum are of the same order or smaller than the standard deviation in all but one case.

A plot of the Stokes'-corrected Fourier coefficients of the 111 and 222 platinum peaks from catalyst 7.1-SiO_2-PtCl-S is given in Fig. 1. These clearly do not superimpose indicating that there are microstrains present. A value for $\langle \epsilon_L^2 \rangle^{\frac{1}{2}}$ of 3×10^{-3} was found at $L = 50$ Å, in the ⟨100⟩ direction. This value corresponds to a dislocation density (ρ) of $\approx 4 \times 10^{15}/m^2$. [This density is calculated from an equation of the form of $\rho = K_{hkl}\langle \epsilon_L^2 \rangle_{hkl}/a_0^2$ where K_{hkl} has been evaluated (*31*).] This corresponds to ≈8–10 dislocations per crystallite of Pt.

In Fig. 2 are the Stokes'-corrected Fourier coefficients of the 111 and 222 platinum peaks from 27-SiO_2-IonX-S. In this case, these clearly superimpose indicating that there is no strain. This was also the case in the ⟨100⟩ direction for this catalyst and for all others examined (in both directions).

The particle sizes in different crystallographic directions from the Fourier analysis of platinum peaks are given in Table 4. Comparison with Table 1 indicates that all catalysts were equiaxed or near spherical except for the first, 7.1-SiO_2-PtCl-S, which appears to be bounded by specific planes. The pattern of sizes is qualitatively similar to that for {110} bounding surfaces. Accordingly, an X-ray value for percentage exposed, D_x could be calculated:[4]

$$D_x = 100 \frac{\text{surface}}{\text{volume}} \times \frac{\rho_S}{\rho_B} = \frac{6 \cdot 100}{\langle L \rangle} \frac{\rho_S}{\rho_B}$$

$$= \frac{11.26}{\langle L \rangle} \times 100, \quad (10)$$

where ρ_S and ρ_B are surface and bulk densities [the former being taken as the average for (111), (100), and (110) planes]. These values are given in column 5 of Table 4 and compared to those determined in Part I (*7*) by hydrogen chemisorption, D_h, in column 6. The agreement is generally excellent, indicating that the crystallites are indeed the Pt particles themselves and will be referred to as such henceforth.

The size distributions for those catalysts without strain are given in Figs. 3–5.

In Fig. 6 the mean square amplitudes of vibration are plotted vs percentage exposed. The value for the bulk ($D_x = 0$) is from the work of Harris *et al.* (*32*) and that for $D_x = 100\%$ is for the free surface as determined by Lyon and Somorjai (*33*). The error bars on three of the points are the standard deviations in a linear-least squares analysis. (The correlation coefficients were 0.68–0.96.) However, these

[4] Smith (*9*) has pointed out that the size measured by Fourier analysis is surface weighted average, not the volume average obtained from integral breadths. Therefore the results from Eq. (10) can be directly compared to the results from gas adsorption techniques.

error bars are probably excessive because: (a) the measurements were repeated on a second specimen and the result was within 8% of that reported in Fig. 6; and (b) the 220 peak from catalyst 27-SiO_2-IonX-S was measured at room temperature and at 77°K. The ratio of integrated intensity at 77°K to that at room tempera-

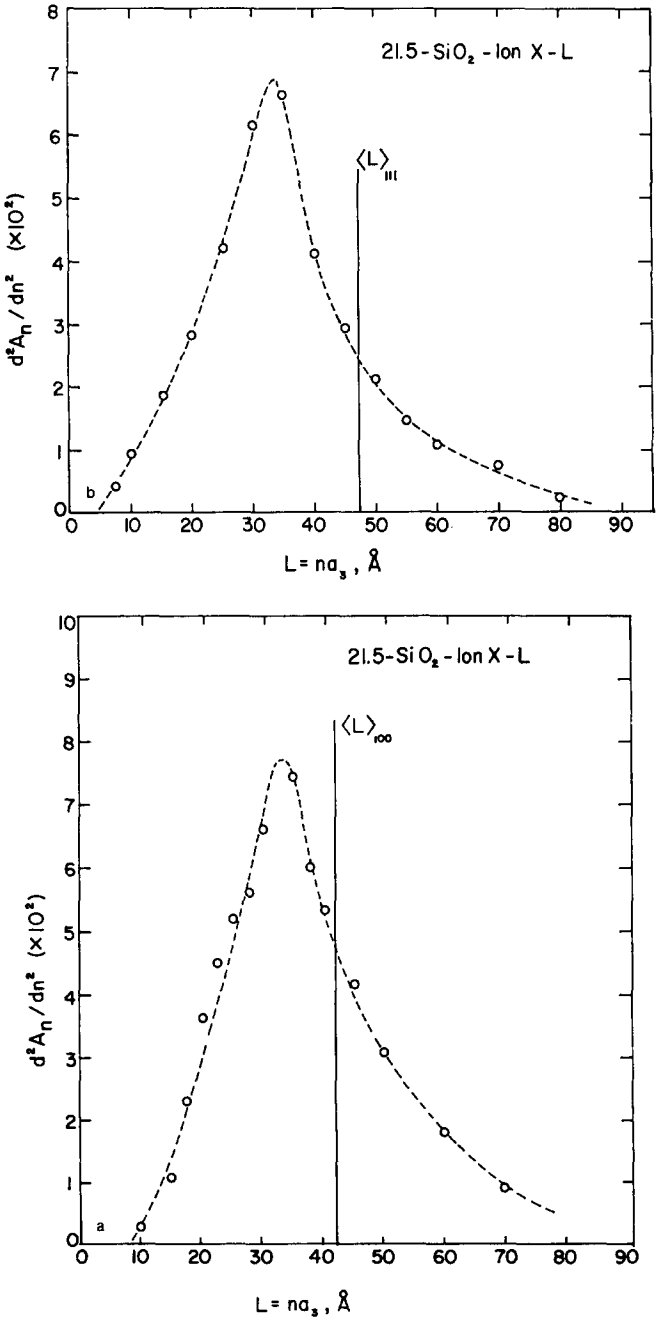

FIG. 5. Particle size distributions for catalyst 21.5-SiO_2-IonX-L. (a) ⟨111⟩ direction, (b) ⟨100⟩ direction, (c) ⟨311⟩ direction.

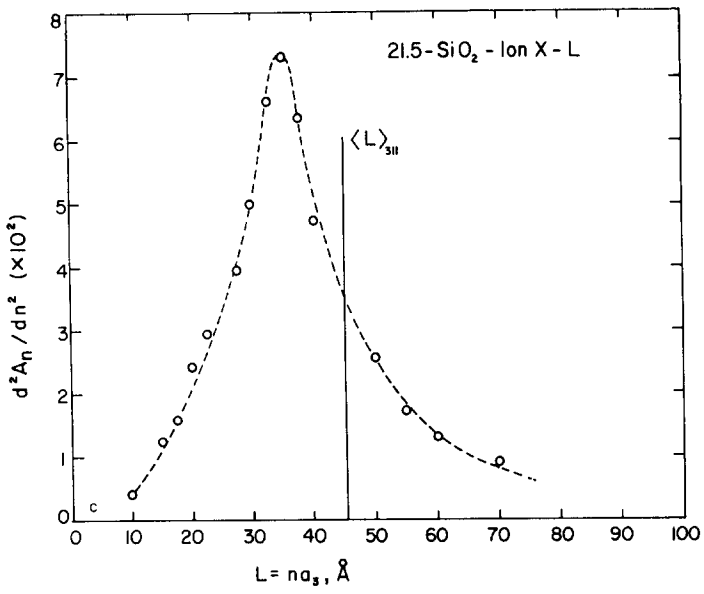

FIGURE 5 (*Continued*)

ture was 1.21, while the expected value was 1.12. The ratio would have been 1.03 if the mean-square vibrational amplitude was that of the bulk. This clearly indicates the rms vibrations are larger for the catalyst than for the bulk.

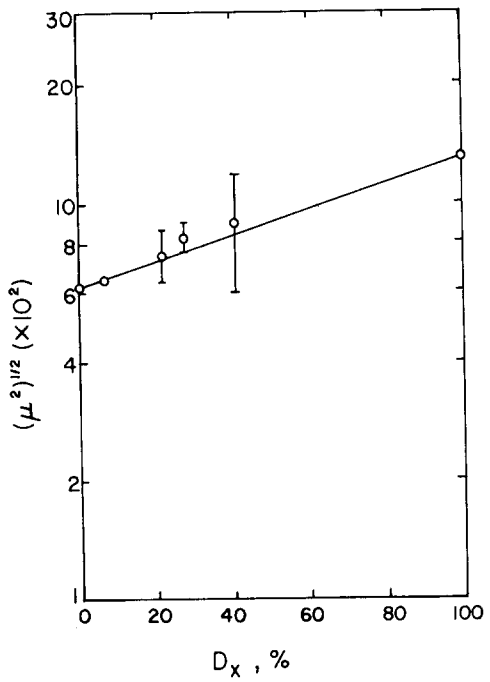

FIG. 6. RMS vibrational amplitude, $\langle\mu^2\rangle^{\frac{1}{2}}$(Å) vs D_x. The value for bulk platinum is from ref. (*32*), that for the free face surface (D_x = 100%) is from ref. (*33*). The line simply connects the end points.

DISCUSSION

The surface area of the gel measured by small-angle X-ray scattering in this study is in good agreement with that determined in Part I by gas adsorption, especially when it is recognized that the procedures for the adsorption techniques are somewhat empirical. Much less care in handling of the samples is required for the X-ray method. With modern rotating anode X-ray generators and position-sensitive detectors (that "see" the entire scattering pattern at once) these measurements can be made completely automatically in 10–30 min. There is, of course, a large capital investment involved, which is not required for the gas adsorption techniques.

Only when the platinum particles are of the same size as the pores in the gel does there appear to be considerable microstrain in the platinum, and in this case the particles are not equiaxed. The microstrains may arise due to the difficulty in

forming the particles in such a case, or due to distortions inherited from the calcining operations due to the differential contraction of the gel and product of the calcination. Further work with different pore and particle sizes is underway to verify this conclusion.

For the other catalysts, the particles are strain free. Even up to 40% fraction exposed, the diffraction pattern is that of platinum indicating that the oxygen present is covering the particles not distorting the internal structure. The particles are relatively equiaxed or nearly spherical. This latter point is indicated by the similar sizes measured in several crystallographic directions and from the size distributions in the ⟨100⟩ and ⟨111⟩ directions. These show a maximum, which would not be the case if the particles were in the form of cubes or tetrahedra, as shown by Smith (*9*). The distributions themselves are interesting. They are sharper for the catalysts formed by impregnation compared to those prepared by ion exchange. Also all the distributions "tail" to large sizes. This indicates (*18*) that the distribution arises due to coagulation of some surface species during preparation rather than by Ostwald ripening.

The platinum particles are also relatively free of stacking faults and microtwins in agreement with studies by electron microscopy (*34*). Sizes down to ≈25 Å have been measured in this study, and there seems to be no reason why even smaller sizes cannot be examined, in controlled environments, with the high X-ray intensities available from modern rotating anode generators, or from a synchrotron. Such studies are now underway. The good agreement between the percentage exposed from these sizes, D_x, and from hydrogen chemisorption, D_h, indicates that the particles are essentially single crystals and, furthermore, that proper line-broadening techniques can be utilized to measure the quantity, D. Again, the initial equipment is expensive, but the measurements are readily automated and careful handling of the specimens is not required.

To within ≈0.1% there is no significant change in the lattice parameter for the oxygen-covered platinum employed in this study over the size range covered, certainly not the order of 0.3–0.7% which has been reported for thin films of gold and silver (*35*, *36*).

The root-mean square amplitudes of vibration have been examined for Au particles of 60 Å (*37*) and tungsten particles of 30 Å (*38*) by the Mössbauer method. For the former an increase was found, while for the latter there was a (13%) decrease compared to the bulk. Harada *et al.* (*39*) examined Au particles of 220 and 250 Å prepared by evaporation and found considerably larger effects than those reported here but for much larger particles; for 120 Å particles, $\langle\mu^2\rangle^{\frac{1}{2}}$ almost doubled. However, there was no indication of the details of the correction for background, and on making measurements vs temperature the authors found no difference from the bulk. They suggested the effect was therefore due to static displacements presumably due to imperfections in the particles. There were no such defects in the particles studied here, and despite the large errors inherent in this kind of measurement, the results in this study clearly extrapolate to the value reported by Lyon and Somorjai for a free surface (*33*). Correlations of these displacements with catalytic activity are made in Part III of this study (*8*).

ACKNOWLEDGMENTS

Surface areas were determined by Mr. J. Solomon in our laboratory. This work was supported through the Materials Research Center of Northwestern University by the Advanced Research Projects Agency of the Department of Defense, Grant No. DAHC-15-73G19.

REFERENCES

1. Whyte, T. E., Jr., *Catal. Rev.*, **8**, 117 (1973).

2. Wagner, C. N. J., *in* "Local Atomic Arrangements Studied by X-Ray Diffraction" (J. B. Cohen and J. E. Hilliard, Eds.), p. 264. Gordon and Breach, New York, 1966.
3. Pearce, C. E., and Lewis, D., *J. Catal.* **26**, 318 (1972).
4. Renouprez, A., Hoang-Van, C., and Compagnon, P. A., *J. Catal.* **34**, 411 (1974).
5. Warren, B. E., "X-Ray Diffraction," p. 251. Addison-Wesley, Reading, Mass., 1969.
6. Mikkola, D. E., and Cohen, J. B., *in* "Local Atomic Arrangements Studied by X-Ray Diffraction" (J. B. Cohen and J. E. Hilliard, Eds.), p. 289. Gordon and Breach, New York, 1966.
7. Uchijima, T., Herrmann, J. M., Inoue, Y., Burwell, R. L., Jr., Butt, J. B. and Cohen, J. B., *J. Catal.* **50**, 464 (1977).
8. Otero-Schipper, P. H., Wachter, W. A., Butt, J. B., Burwell, Jr., R. L., and Cohen, J. B., *J. Catal.* **50**, 494 (1977).
9. Smith, W. L., *J. Appl. Crystallogr.* **5**, 127 (1972).
10. Pausescu, P., Manaila, R., Popescu, M., and Jijovici, E., *J. Appl. Crystallogr.* **7**, 281 (1974).
11. Das, B. N., Sarney-Loomis, A. D., Wald, F., and Wolff, G. A., *Mater. Res. Bull.* **3**, 649 (1968).
12. Cohen, J. B., and Schwartz, L. H., "Diffraction from Materials." Academic Press, New York, (1977).
13. De Angelis, R. J., *in* "Local Atomic Arrangements Studied by X-Ray Diffraction" (J. B. Cohen and J. E. Hilliard, Eds.), p. 271. Gordon and Breach, New York, 1966.
14. Stokes, A. R., *Proc. Phys. Soc. London* **61**, 382 (1948).
15. Kidron, A., and Cohen, J. B., *J. Appl. Crystallogr.* **6**, 8 (1973).
16. Rothman, R. L., and Cohen, J. B., *Advan. X-Ray Anal.* **12**, 208 (1969).
17. Gangulee, A., *J. Appl. Crystallogr.* **7**, 434 (1974); Mignot, J., and Rondot, D., *Acta Met.* **23**, 1321 (1975).
18. Granqvist, C. G., and Buhrman, R. A., *J. Catal.* **42**, 477 (1976).
19. Smith, W. L., *J. Appl. Crystallogr.* **9**, 187 (1976).
20. Mikkola, D. E., and Cohen, J. B., *Acta Met.* **14**, 105 (1966).
21. Cohen, J. B., and Wagner, C. N. J., *J. Appl. Phys.* **33**, 2073 (1962).
22. Chipman, D. R., and Walker, C. B., *Acta Crystallogr.* **A28**, 572 (1972).
23. "International Tables for X-Ray Crystallography" (J. A. Ibers and W. C. Hamilton, Eds.), Vol. 4. Kynoch Press, Birmingham, England, 1974.
24. Pearson, W. B., "Handbook of Lattice Spacings and Structure of Metals and Alloys," Pergamon Press, New York, 1958.
25. McFarlane, R. E., Rayne, J. A., and Jones, C. K., *Phys. Lett.* **18**, 91 (1965).
26. "Small Angle Scattering" (H. Brumberger, Ed.), Part 6. Gordon and Breach, New York, 1967.
27. Richesson, M., Morrison, L. Cohen, J. B., and Paavola, K., *J. Appl. Crystallogr.* **4**, 524 (1971).
28. Kratky, O., *in* "Small Angle Scattering" (H. Brumberger, Ed.), p. 63. Gordon and Breach, New York, 1967.
29. De Angelis, R. J., and Cohen, J. B., *in* "Deformation Twinning" (R. E. Reed-Hill, J. P. Hirth, and H. C. Rogers, Eds.), p. 430. Gordon and Breach, New York, 1964.
30. Nelson, J. B., and Riley, D. P., *Proc. Phys. Soc. London* **57**, 477 (1945).
31. Otte, H., *J. Appl. Phys.* **38**, 217 (1967).
32. Harris, J. R., Benczer-Koller, N., and Rothberg, G. M., *Phys. Rev.* **137**, A1101 (1965).
33. Lyon, H. B., and Somorjai, G. A., *J. Chem. Phys.* **44**, 3707 (1966).
34. Avery, N. R., and Sanders, J. B., *J. Catal.* **18**, 129 (1970).
35. Mays, C. W., Vermaak, J. S., and Kuhlmann-Wilsdorf, D., *Surface Sci.* **12**, 134 (1968).
36. Wasserman, H. J., and Vermaak, J. S., *Surface Sci.* **22**, 164 (1970).
37. Marshall, S. W., and Wilenzick, R. M., *Phys. Rev. Lett.* **16**, 219 (1966).
38. Roth, S., and Horl, E. M., *Phys. Lett.* **A25**, 299 (1967).
39. Harada, J., Yao, S., and Ichimiya, A., *in* "10th International Congress of Crystallography," August 7–15, 1975. Abstract 13.2-6.